International Journal of Fracture **93:** 315–333, 1998.
© 1998 *Kluwer Academic Publishers. Printed in the Netherlands.*

Interface strength, work of adhesion and plasticity in the peel test

YUEGUANG WEI and JOHN W. HUTCHINSON
Division of Engineering and Applied Sciences, Harvard University, Cambridge, MA 01238, USA
e-mail: hutchinson@husm.harvard.edu

Received 23 October 1997; accepted in revised form 3 September 1998

Abstract. A cohesive zone model is proposed and analyzed for steady-state peeling of a thin rate-independent, elastic-plastic film bonded to an elastic substrate. A traction-separation description of the interface is embedded within continuum characterizations of the film and substrate. The primary parameters characterizing the traction-separation relation are the work of adhesion and the peak separation stress, termed the interface strength. The objective of the study is the determination of the relationship of the peel force to the work of adhesion of the interface and its strength, with due regard for plastic deformation in the film. An example of an elastic film peeled from an elastic-plastic substrate is also presented.

Key words: Peel test, work of adhesion, interface strength, plastic yielding, adhesion of thin films.

1. Introduction

The study of the peel test conducted in this paper continues efforts by Kim and Kim (1988), Kim and Aravas (1988) and, most recently by Kinlock, Lau and Williams (1994) to characterize the mechanics of the test. Earlier work on this topic is cited in these papers. One of the primary aims of this general line of research has been to link the peel force or, equivalently, the macroscopic work of fracture, to the work of interface adhesion by accounting for plastic deformation accompanying the peeling process. In steady-state peeling, the peel force per unit width of film is simply related to the macroscopic work of fracture, which is effectively the sum of the work of adhesion and the plastic dissipation. Successful partitioning of these two contributions to the peel force would enable the work of adhesion to be inferred. Here, the research is carried one step beyond the previous studies. A cohesive zone model is introduced wherein a traction-separation relation is employed to model the interface as a condition linking continuum descriptions of the film and the substrate. The traction-separation relation is characterized by the work of adhesion (energy per unit area) Γ_0 and a maximum separation stress $\widehat{\sigma}$ which can be regarded as the interface strength under normal stressing. Under steady-state conditions, the model provides the peel force per unit width of the film P in terms of Γ_0, $\widehat{\sigma}$, the properties of the film and substrate, and the peel angle Φ. With one exception, the paper deals with elastic-plastic films bonded to elastic substrates.

When conditions are such that negligible plastic deformation occurs, the simple work balance $P(1 - \cos\Phi) = \Gamma_0$ holds, independent of $\widehat{\sigma}$, assuming the stretch energy in the film can be neglected. Perhaps it is for this reason that prior work has not focused on the role of interface strength in the mechanics of the peel test. When plastic deformation does occur, the extent to which $P(1 - \cos\Phi)$ exceeds Γ_0 depends strongly on $\widehat{\sigma}$. The two-parameter characterization $(\Gamma_0, \widehat{\sigma})$ of the interface in the present model has a parallel in the approach adopted by Kim and Kim (1988), Kim and Aravas (1988), and Kinloch et al. (1994) wherein

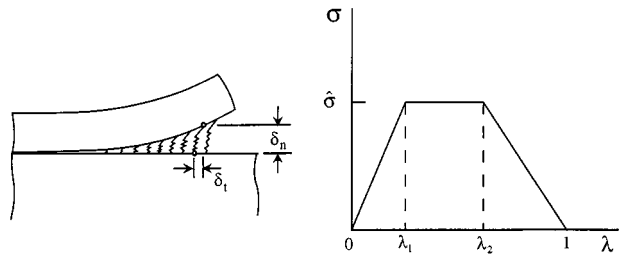

Figure 1. Traction-separation relation governing separation of the interface.

both the work of adhesion and an opening angle where the film leaves the substrate are used as parameters to specify the peeling process. Further discussion emphasizing contrast between the two approaches will be given later in the paper.

The traction-separation relation of the interface is postulated in Section 2, following earlier work on general interface fracture by Tvergaard and Hutchinson (1993). A complete specification of the model follows in Section 3. Details of the numerical method for steady-state peeling are given in Section 4, and numerical results are presented in Section 5. Conclusions, limitations of the model, and recommendations for further work are given in Section 6.

2. The interface traction-separation relation

The thickness of the interface in the unloaded state is taken to be zero. Following the notation for the interface traction-separation relation introduced in Tvergaard and Hutchinson (1993), let δ_n and δ_t be the normal and tangential components of the relative displacement of the respective faces across the interface in the zone where the separation process occurs, as indicated in Figure 1. Let δ_n^c and δ_t^c be critical values of these displacement components, and define a single dimensionless separation measure as

$$\lambda = \sqrt{(\delta_n/\delta_n^c)^2 + (\delta_t/\delta_t^c)^2}, \tag{2.1}$$

such that the tractions drop to zero when $\lambda = 1$. With $\sigma(\lambda)$ displayed in Figure 1, a potential from which the interface tractions in the separation zone are derived is defined as

$$\Pi(\delta_n, \delta_t) = \delta_n^c \int_0^\lambda \sigma(\lambda')\,\mathrm{d}\lambda'. \tag{2.2}$$

The normal and tangential components of the traction acting across the interface in the fracture process zone are given by

$$T_n = \frac{\partial \Pi}{\partial \delta_n} = \frac{\sigma(\lambda)}{\lambda}\frac{\delta_n}{\delta_n^c}, \qquad T_t = \frac{\partial \Pi}{\partial \delta_t} = \frac{\sigma(\lambda)}{\lambda}\frac{\delta_t}{\delta_t^c}\frac{\delta_n^c}{\delta_t^c}. \tag{2.3}$$

The traction law under a purely normal separation ($\delta_t = 0$) is $T_n = \sigma(\lambda)$ where $\lambda = \delta_n/\delta_n^c$. The peak normal traction under purely normal separation is $\widehat{\sigma}$, which will be termed the interface strength. Under a purely tangential displacement ($\delta_n = 0$), $T_t = (\delta_n^c/\delta_t^c)\sigma(\lambda)$ where $\lambda = \delta_t/\delta_t^c$. The peak shear traction is $(\delta_n^c/\delta_t^c)\widehat{\sigma}$ under a purely tangential displacement

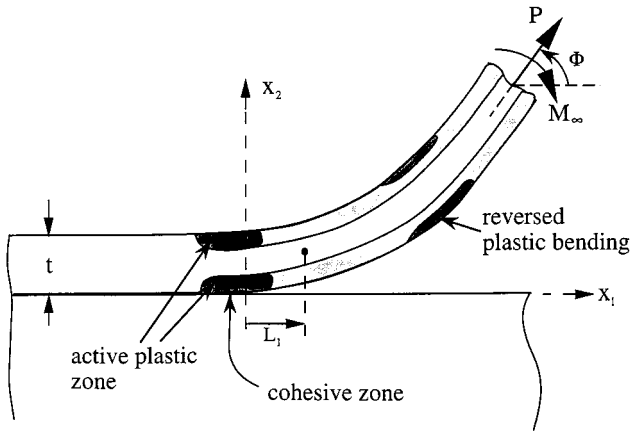

Figure 2. Model of steady-state peeling. A plane strain finite element formulation is used to produce the solution for the substrate and the portion of the film to the left of $x_1 = L_1$. An elastic–plastic 'elastica' solution is applied for the portion of the film to the right of $x_1 = L_1$.

of the faces. The work of separation per unit area of interface Γ_0 is given by (2.2) with $\lambda = 1$. For the separation function $\sigma(\lambda)$ specified in Figure 1

$$\Gamma_0 = \tfrac{1}{2}\widehat{\sigma}\delta_n^c[1 - \lambda_1 + \lambda_2]. \tag{2.4}$$

The separation law is assumed to be independent of the time rate of deformation, as are the constitutive models characterizing the film and substrate. The parameters governing the separation law of the interface are the work of the fracture process Γ_0, the peak stress quantity $\widehat{\sigma}$, and the critical displacement ratio δ_n^c/δ_t^c, together with the factors λ_1 and λ_2 governing the shape of the separation function. Use of the potential ensures that the work of separation is Γ_0 regardless of the combination of normal and tangential displacements taking place in the separation of the interface. Experience gained in the earlier studies suggests that details of the shape of the separation law are relatively unimportant. The two most important parameters characterizing interface separation are Γ_0 and $\widehat{\sigma}$. The parameter δ_n^c/δ_t^c is the next most important, but the study of mixed mode interface toughness (Tvergaard and Hutchinson, 1993) indicates that predictions are relatively insensitive to this parameter as long as the interface process is dominantly normal separation. This is the case for the peel test under the range of peel angles considered here.

Attainment of $\lambda = 1$ at the end of the traction-separation zone is the condition for crack advance. In steady-state propagation, this condition must be imposed on the solution.

3. An embedded cohesive zone model for steady-state peeling

The geometry of the model is displayed in Figure 2 with a peel angle Φ. Plane strain conditions are assumed, as appropriate for a film whose width normal to the plane of deformation in Figure 2 is sufficiently large compared to its thickness t. Except for one example presented at the end of the paper, the film is taken to be elastic–plastic with Young's modulus E, Poisson's ratio ν, tensile yield stress σ_Y, and strain hardening exponent N. Rate-independent material behavior is assumed. The substrate is elastic with modulus E_s and Poisson's ratio ν_s. The standard J_2 flow theory of plasticity, based on the von Mises yield surface, is used to characterize plasticity in the film. The small strain version of the theory is employed, consistent

with the fact that the strains and rotations at the tip of the steadily growing crack are indeed small under steady-state conditions. The tensile stress-strain relation used to characterize the film material is

$$\begin{aligned} \varepsilon &= \sigma/E \quad \text{for } \sigma \leqslant \sigma_Y, \\ &= (\sigma_Y/E)(\sigma/\sigma_Y)^{1/N} \quad \text{for } \sigma > \sigma_Y. \end{aligned} \tag{3.1}$$

The interface crack is assumed to have propagated a sufficient distance such that steady-state conditions prevail in the vicinity of the propagating interface crack. In Figure 2, the interface crack propagates to the left. The active plastic zone where the plastic strain rate $\dot{\varepsilon}_{ij}^p$ is nonzero is depicted by dark shading. Zones behind the advancing tip which have unloaded but which contain residual plastic strains are shown by light shading. Zones of reversed plastic loading will generally occur at some distance from the crack tip in the detached the film strip (Kim and Aravas, 1988; Kinlock et al., 1994), and these are also depicted by dark shading.

The peel angle Φ specifies the angle which the peel force per unit width of film P makes with the plane of the interface. Let $M(s)$ be the bending moment (per unit width) about the middle plane of the separated film at a distance s along the film measured from the crack tip. Take the origin of the coordinate system (x_1, x_2) at current location of the tip where $\lambda = 1$. For analysis purposes, the problem is sub-divided into two parts (cf. Figure 2): the substrate plus the film to the left of $s = x_1 = L_1$, and the separated infinite film segment to the right of L_1. Accurate results from the cohesive zone model require a full 2D plane strain, continuum analysis of the behavior in the vicinity of the interface crack. Representation of the film and substrate by a beam model of the film in the vicinity of the separation zone misses essential features of the phenomena. For example, the small scale yielding limit when the active plastic zone is confined to a region near the crack tip cannot be captured by a beam model. An Eulerian-based, finite element formulation designed to cope with steady-state conditions will be employed for this part of the problem. The point at $s = L_1$ is where the full 2D continuum analysis of the crack tip problem is matched to a 1D bending problem for the separated film strip. This point must lie to the right of the active plastic zone at the crack tip and to the left of any reversed plastic bending. Otherwise, the location of this matching point will be seen to have essentially no effect on the solution as long as the slope there θ_1 is small.

The film which emerges from the region to the left of L_1 has been subject to plastic deformation and has a residual curvature κ_0 prior to any reversed plastic deformation. The residual curvature κ_0 is computed as part of the solution to the crack tip problem. The film at the matching point $s = L_1$ has undergone elastic unloading sustaining a moment M_1 less than the maximum moment, which is attained at some point to the left of L_1. The moment-curvature relation of the film emerging into the region to the right of L_1 is displayed as the unloading branch in Figure 3. The initial portion of the curve of M versus κ is shown dashed since it is not used in the analysis. (This is the portion of the behavior computed using the full 2D representation of the film.) Reversed plastic deformation, if it occurs, takes place when M becomes sufficiently negative (Kim and Kim, 1988; Kim and Aravas, 1988; Kinlock et al., 1994). At distances s which are far from the tip the film becomes straight, corresponding to the state $M = -M_\infty$ with $\kappa = 0$. The final residual curvature of the *unloaded* film ($M = 0$) is labeled in Figure 3 as κ_f.

Plastic deformation due to reversed plastic bending contributes to the overall rate of plastic work in the system, and it reduces the final residual curvature of the film from the value, κ_0, inherited from the plastic deformation in the vicinity of the interface crack tip. Reversed plastic deformation depends on the Bauschinger behavior of the material, which is not well

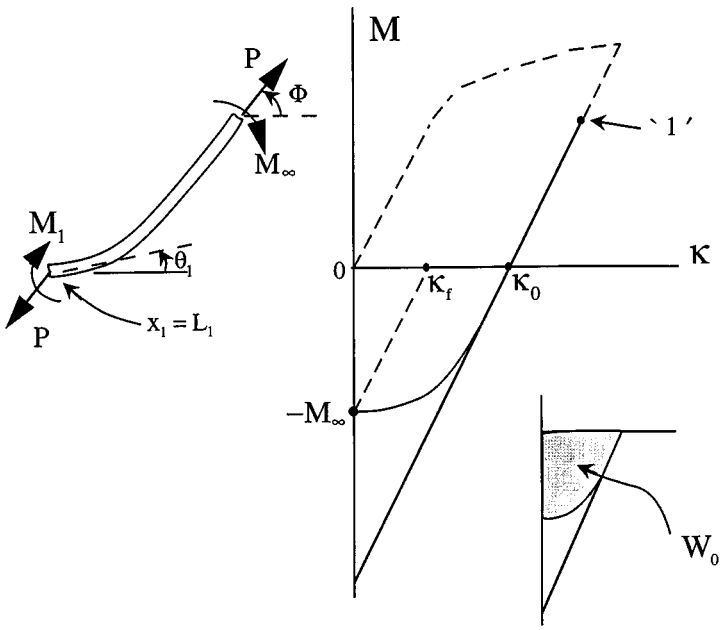

Figure 3. Moment-curvature relation governing behavior of the film to the right of $x_1 = L_1$.

quantified by conventional yield surface descriptions, especially not by an isotropic hardening theory. Because reversed plastic deformation occurs in the segment of the problem which is well characterized by 1D nonlinear bending theory, full details of the plastic constitutive behavior under reversed loading need not be considered. It will be shown that only the shaded area W_0 under the overall moment-curvature relation of the film in Figure 3 matters in the final results.

The study in this paper will consider the following parameters

$$E, \nu, \sigma_Y, N, t \ \text{(film)}; \quad E_s, \nu_s \ \text{(substrate)}; \quad \Gamma_0, \widehat{\sigma} \ \text{(interface)}. \tag{3.2}$$

The peel angle Φ and the work per unit width of film W_0 characterizing reversed plastic bending complete the parameter set. An additional variable which is likely to have a major influence on the peel force is residual stress in the attached film acquired in the bonding process. When the residual stress is a nonnegligible fraction of the yield stress, it will alter the plastic dissipation. Residual prestress can be included in the model, but it will not be considered in this paper in the interest of reducing the number of variables.

The following material-based length quantity plays a fundamental role in the solution

$$R_0 = \frac{1}{3\pi(1-\nu^2)} \frac{E\Gamma_0}{\sigma_Y^2}. \tag{3.3}$$

The extent of the plastic zone scales with R_0. When P is only slightly larger than Γ_0, this length can be regarded as a estimate of the plastic zone height in the film at the crack tip (Tvergaard and Hutchinson, 1992, 1993). In general, however R_0 is less than the plastic zone height and should simply be regarded as a fundamental parameter with dimensions of length. The same length quantity (apart from a numerical constant) emerges as fundamental in the

analysis of Kim and Kim (1988). Dimensional considerations dictate that the solution for the peel force P must have the general nondimensional form

$$\frac{P}{\Gamma_0} = F\left\{\frac{t}{R_0}, \frac{\widehat{\sigma}}{\sigma_Y}, N, \Phi, \frac{\sigma_Y}{E}, \frac{E_s}{E}, \nu, \nu_s\right\}, \tag{3.4}$$

where F is dimensionless. Implicit in this dependence are details of the hardening rule for reversed plastic straining, e.g. isotropic vs. kinematic hardening. The number of dimensionless variables in any mechanics model of the peel test is large, even when any residual stress arising during bonding is ignored. To reduce the number of variables, most of the calculations in the present study will be made with $\nu_s = \nu = 0.3$, and with either no elastic mismatch ($E_s = E$) or for a highly compliant film on a stiff substrate with $E = E_s/100$. The shape parameters in the traction separation law are taken to be $\lambda_1 = 0.15$ and $\lambda_2 = 0.5$, while δ_n^c/δ_t^c is fixed at 1. Of the remaining dimensionless variables in (3.4), t/R_0, $\widehat{\sigma}/\sigma_Y$, N and Φ all have significant influence on P/Γ_0 when plastic dissipation is nonnegligible.

In steady-state peeling, the work done by the peel force per unit advance of the interface crack (per unit width of film) is $P(1-\cos\Phi)$. This assumes the contribution of overall stretch energy of the film (including residual elastic energy in the bonded film) to the work balance can be neglected. Thus, $P(1-\cos\Phi)/\Gamma_0$ represents the ratio of the total work of fracture to the work of interface adhesion, while $P(1-\cos\Phi) - \Gamma_0$, represents the plastic dissipation in steady-state peeling.

4. Formulation and numerical solution

The two parts of the problem in Figure 2 are analyzed separately and coupled by requiring continuity of force, moment, displacement and rotation at $x_1 = L_1$. The first part to the left of L_1 is analyzed as a steady-state, plane strain continuum problem. The second part to the right of L_1 is treated as a finite rotation, bending problem (an elastic–plastic 'elastica') with a residual curvature κ_0 arising from plastic deformation in the first part. The analysis of each part is described, followed by a prescription of the coupling conditions.

4.1. Finite element solution for the first part of the problem

The stresses and strains well ahead of the advancing interface crack tip ($x_1 \to -\infty$) vanish because residual stresses in the film are assumed to be absent. In the small strain, small rotation steady-state problem, the rate at any point of a quantity such as stress or strain is related to the leftward velocity V of the crack tip and the gradient in the x_1 direction by

$$\dot{\varepsilon}_{ij} = V\partial\varepsilon_{ij}/\partial x_1. \tag{4.1}$$

It is this feature which makes it possible to directly solve the problem without having to consider transient behavior preceding attainment of steady-state. The Eulerian-based solution scheme was developed by Dean and Hutchinson (1980) and Parks, Lam and McMeeking (1981). It was applied to a related study of steady-state thin film delamination by Wei and Hutchinson (1997a). In outline, it is as follows.

Anticipating numerical implementation within a finite element framework, let E be the strain vector with components comprising the strains, and let Σ be the stress vector containing components of stress. Denote the plastic strain vector by E^p. The matrix of incremental moduli for plastic loading is denoted by $\mathbf{D}$ such that $\dot{\Sigma} = \mathbf{D}\dot{E}$; the corresponding elastic matrix of

moduli is denoted by $\mathbf{D}^e$. The solution employs iteration. In each iteration, the core procedure is the finite element solution for the displacements, strains and stresses *assuming that the plastic strain distribution E^p is known*. In notation standard to the finite element method, let $\mathbf{U}$ be the vector of nodal displacements and let $\mathbf{B}$ be the strain matrix such that $E = \mathbf{BU}$. The finite element problem for $\mathbf{U}$ in terms of applied boundary forces $\mathbf{F}$ (distributions matching P and M are prescribed at $x_1 = L_1$) and any specified E^p is represented in the standard notation as

$$\mathbf{K}^e\mathbf{U} = \int_S \mathbf{N}^T\mathbf{F}\,\mathrm{d}S + \int_V \mathbf{B}^T\mathbf{D}^e\mathbf{E}^p\,\mathrm{d}V \quad \text{where } \mathbf{K}^e = \int_V \mathbf{B}^T\mathbf{D}^e\mathbf{B}\,\mathrm{d}V. \tag{4.2}$$

The iteration steps are as follows

(1) Use the distribution of E^p from the previous iteration in (4.2) to determine $\mathbf{U}$. In the first iteration take $E^p = \mathbf{0}$.
(2) Compute $\mathbf{E}$ from $\mathbf{U}$.
(3) Obtain a new estimate of the distribution of Σ. Use $\Sigma = \mathbf{D}^e\mathbf{E}$ in the region upstream of the current estimate of active plastic zone and use $\Sigma = \mathbf{D}^e(\mathbf{E} - E^p)$ downstream from the active zone. Where yield is currently met, make use the fact that for steady-state growth, $\dot{\Sigma} = \mathbf{D}\dot{E}$ can be replaced by $\partial\Sigma/\partial x_1 = \mathbf{D}\,\partial\mathbf{E}/\partial x_1$ such that for any point (x_1, x_2) within the active plastic zone

$$\Sigma(x_1, x_2) = \Sigma(x_1^*, x_2) - \int_{x_1}^{x_1^*} \mathbf{D}\,\partial\mathbf{E}/\partial x_1\,\mathrm{d}x_1, \tag{4.3}$$

where (x_1^*, x_2) is corresponding point on the leading edge of the active plastic zone (i.e., the left edge of the active zone). The integration in (4.3) is performed for fixed x_2 and applies to all points within the active plastic zone.
(4) Use $\mathbf{E}^p = \mathbf{E} - \mathbf{D}^{e^{-1}}\Sigma$ to compute the new estimate of $\mathbf{E}^p$ for the next iteration. Revise the boundaries of the active plastic zone using the new estimate of Σ. To the right of the active plastic zone in the downstream unloading region, $\mathbf{E}^p$ is a function only of x_2, corresponding to its value at the right edge of the active zone.
(5) If satisfactory convergence has not been achieved repeat steps (1) through (4).

Isoparametric elements with nine nodes with 2×2 Gauss integration are employed in the formulation. The traction-separation relation (2.3) is imposed on (4.2) by converting the tractions T_t and T_n to boundary forces linked to the displacement jumps across the crack face. These nonlinear equations are solved as part of the iterative process. The criterion for continuing crack propagation (i.e., $\lambda = 1$ at the end of the cohesive zone), is imposed on the solution.

4.2. Solution in the second part of the film in $s > L_1$

Within the first part, the film emerges from the active plastic zone with a plastic strain $\varepsilon_{ij}^p(x_2)$ which depends on x_2 but is independent of x_1. This is the state inherited by the film segment to the right of L_1. If the film were unloaded prior to any reversed plastic bending, it would have a residual curvature κ_0 given by

$$\kappa_0 = -\frac{12}{t^3}\int_0^t (x_2 - \tfrac{1}{2}t)\varepsilon_{11}^p(x_2)\,\mathrm{d}x_2 \tag{4.4}$$

which is computed from the solution to the first part. As noted earlier, reversed plastic deformation further to the right of L_1 will reduce the final residual curvature of the unloaded peeled film to κ_f.

The film segment to the right of L_1 is modeled as an inextensional elastic-plastic 'elastica', following earlier approaches. In this segment, the relation of the moment per unit width M and curvature κ is of the form shown in Figure 3. During unloading prior to reversed plastic bending, $M = B(\kappa - \kappa_0)$, where $B = Et^3/[12(1-\nu^2)]$ is the elastic bending stiffness per unit width of the film. With s as the distance along the film middle surface measured from the tip, and with θ as the rotation of the film middle surface relative to the x_1-axis, $\kappa = \mathrm{d}\theta/\mathrm{d}s$. Equilibrium requires $\mathrm{d}M/\mathrm{d}s = -P\sin(\Phi - \theta)$. By $\kappa = \mathrm{d}\theta/\mathrm{d}s$, the equilibrium equation can be rewritten as

$$\kappa\,\mathrm{d}M = -P\sin(\Phi - \theta)\,\mathrm{d}\theta. \tag{4.5}$$

Let M be any moment on the unloading curve in Figure 3 and let θ and κ be associated values. Integrate (4.5) from $M = -M_\infty$, where $\theta = \Phi$ and $\kappa = 0$, to M to obtain

$$W(M) = P[1 - \cos(\Phi - \theta)], \tag{4.6}$$

where $W(M)$ is the area to the right of the M-axis of the unloading moment-curvature curve between $-M_\infty$ and M

$$W(M) = \int_{-M_\infty}^{M} \kappa\,\mathrm{d}M. \tag{4.7}$$

Equation (4.6) provides the connection between M_1 and θ_1 at the point $s = L_1$, i.e.,

$$W(M_1) = P[1 - \cos(\Phi - \theta_1)]. \tag{4.8}$$

It proves to be revealing to bring into play the area $W_0 \equiv W(M = 0)$ of the unloading curve below the κ axis (cf. Figure 3). By (4.6),

$$W_0 = P[1 - \cos(\Phi - \theta_0)], \tag{4.9}$$

where θ_0 is the rotation at the point corresponding to $M = 0$. Subtract (4.9) from (4.8), noting that $W(M_1) - W_0$ is simply $M_1\kappa_0 + M_1^2/(2B)$. The resulting equation can manipulated and solved for M_1

$$M_1 = B\kappa_0\left[\sqrt{[1 - \cos(\Phi - \theta_1)][2P/(B\kappa_0^2)] + 1 - w_0} - 1\right], \tag{4.10}$$

where

$$w_0 = \frac{W_0}{\frac{1}{2}B\kappa_0^2}. \tag{4.11}$$

In this form, it can be seen that the relation between M_1 and θ_1 (which is an exact integration of the nonlinear elastic–plastic bending equation) depends on reversed plastic bending only through the area ratio w_0. As $B\kappa_0^2/2$ is the area below the κ-axis in Figure 3 in unloading

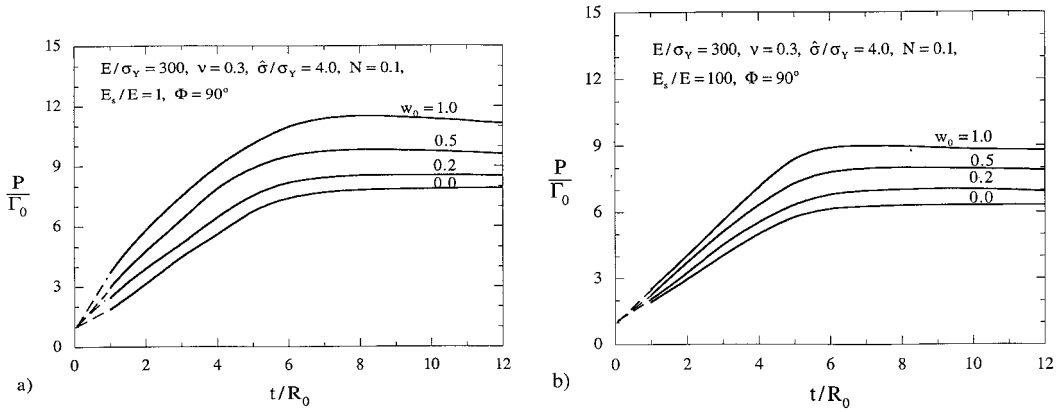

Figure 4. Normalized peeling force P/Γ_0 as a function of normalized film thickness t/R_0 for several values of the parameter characterizing reversed plastic bending w_0. The interface is moderately strong with $\widehat{\sigma}/\sigma_Y = 4$. (a) $E_s/E = 1$. (b) $E_s/E = 100$. Peel force is normal to the interface, $\Phi = 90°$. The other parameters are specified in the figure.

elastically to $\kappa = 0$, w_0 provides a measure of the effect of reversed plastic bending. It will be unity if no reversed plastic bending occurs. Smaller values of this ratio are pertinent when peeling involves significant plastic deformation. The quantity w_0 can be computed for any specific stress-strain description for reversed stressing. However, given the variety of plasticity descriptions for reversed stressing and the lack of agreement on which constitutes the best choice, we prefer to retain w_0 as an independent parameter in our analysis. It will be seen that its role is relatively minor.

4.3. Coupling of two parts of the solution at $s = L_1$

Continuity of displacement, rotation, force and moment are required at the point $s = x_1 = L_1$ where the two parts of the solution are matched. For the problem of the first part, a linear distribution of tractions is applied to the film along $x_1 = L_1$ with resultants chosen to coincide with the horizontal and vertical components of the force per unit width $(P\cos\Phi,\ P\sin\Phi)$ and the moment per unit width M_1. The rotation θ_1 in the first part is computed as the rotation of the centerline of the film at $x_1 = L_1$. The continuity conditions are included in the set of equations to be satisfied in the iterative solution process. Thus, M_1 and θ_1 computed from the first part satisfy (4.10) at the end of the iteration process.

5. Numerical results for steady-state peeling

Calculations have been performed based on the formulation described above, and selected results will be presented in this section to bring out the dependence of the normalized peel force, P/Γ_0, on the dimensionless parameters identified in (3.4). The fraction w_0 measuring the contribution from reversed plastic bending is an additional parameter which will be considered. As emphasized in Section 3, $P(1-\cos\Phi)/\Gamma_0$ represents the ratio of the macroscopic work of fracture to the work of interface adhesion. The extent to which $P(1-\cos\Phi)/\Gamma_0$ exceeds unity reflects the relative contribution of plastic dissipation in the film to the total work of fracture.

5.1. Normal peel force ($\Phi = 90°$)

Curves of P/Γ_0 as a function of the normalized film thickness t/R_0 are shown in Figure 4 for a peeling force acting normal to the interface ($\Phi = 90°$). In Figure 4(a), the elastic modulus of the substrate is identical to that of the film, while in Figure 4(b), the substrate is a hundred times stiffer than the film ($E_s/E = 100$). Otherwise, the parameters characterizing the film and the interface are the same in these two plots. In particular, the interface is taken to be relatively strong with an interface strength $\widehat{\sigma}$ four times the yield strength of the film σ_Y. The strain hardening index of the film is $N = 0.1$. The work of interface adhesion Γ_0 enters as the normalization of the peel force P and also in the length parameter R_0 defined in (3.3). The full range of reversed plastic bending is spanned by the curves in Figures 4(a,b). Recall that $w_0 = 1$ corresponds to no reversed plastic bending. At the other limit $w_0 = 0$ reversed plastic bending occurs as soon as M becomes negative. This latter limit would never be fully attained and would be approached only if the plastic deformation accompanying peeling were large. Suppression of reversed plastic bending has the effect of decreasing the moment carried by the film at the crack tip, thereby requiring a larger peel force to propagate the crack than when reversed plastic bending occurs. It is evident from Figure 4 that reversed plastic bending plays some role in determining the peel force, but not a dominant one. Similarly, a stiff substrate reduces the peel force relative to that for a more compliant substrate, but the effect is not large.

The influence of the location $x_1 = L_1$ where the two parts of the solution described in Section 4 are matched has been explored by repeating the calculations with different choices of L_1 to test for numerical sensitivity. Since the first part of the solution (the finite element solution) is based on a small rotation formulation, it is also essential that θ_1 be small. The calculations reported in this section were computed with $L_1/R_0 = 20$. This choice ensures that the matching point is well ahead of the active plastic zone at the crack tip and well to the left of the zone of reversed plastic bending. The angle θ_1 never exceeds 10°. Repeating selected calculations such as those shown in Figure 4 for other choices of L_1/R_0, differing by as much as a factor of 2, produced at most, only a 2 or 3 percent change in the peel force.

The major trend brought out by Figure 4 is the dependence of the peel force on the film thickness t. Numerical values of P/Γ_0 in Figures 4(a,b) have been computed at all integer values of t/R_0 between 1 and 12. When t is small compared to R_0, plasticity occurs throughout the film, but plastic dissipation is nevertheless small compared to Γ_0 because the volume of film material is small. The peel test is an unusual illustration of a fracture phenomenon where large scale yielding is associated with lower toughness than small scale yielding. In the limit as t goes to zero, P approaches the interface adhesion Γ_0. The dashed sections of the curves between $t/R_0 = 0$ and 1 have been drawn to connect with $P/\Gamma_0 = 1$. At the other limit, when t/R_0 is sufficiently large, P/Γ_0 approaches an asymptote. This asymptote corresponds to a small scale yielding limit in the sense that the active plastic zone is confined to the crack tip, is small compared to the film thickness, and becomes independent of t/R_0. In this limit, there is no yielding on the top surface of the film above the tip and no reversed plastic bending such that $w_0 = 1$. Steady-state toughness in this limit is the same as that for an interface crack in small scale yielding at the same mode mixity (Tvergaard and Hutchinson, 1993).

The relatively strong interface ($\widehat{\sigma}/\sigma_Y = 4$) gives rise to considerable plastic dissipation such that the total work of fracture is approximately an order of magnitude greater than the work of interface adhesion when the film is sufficiently thick. For normalized interface strengths $\widehat{\sigma}/\sigma_Y$ above 4 in Figure 5, the peel force attains a maximum when the normalized thickness is approximately $t/R_0 = 6$ for the case $w_0 = 1$. The peak becomes somewhat

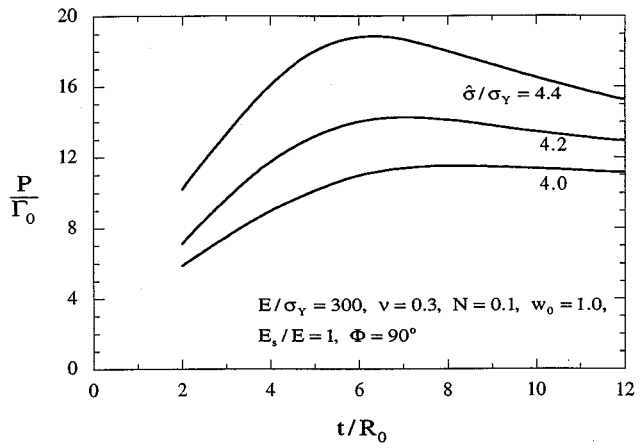

Figure 5. Normalized peeling force P/Γ_0 as a function of normalized film thickness t/R_0 for several values of the normalized interface strength, $\widehat{\sigma}/\sigma_Y$. The peel force is normal to the interface.

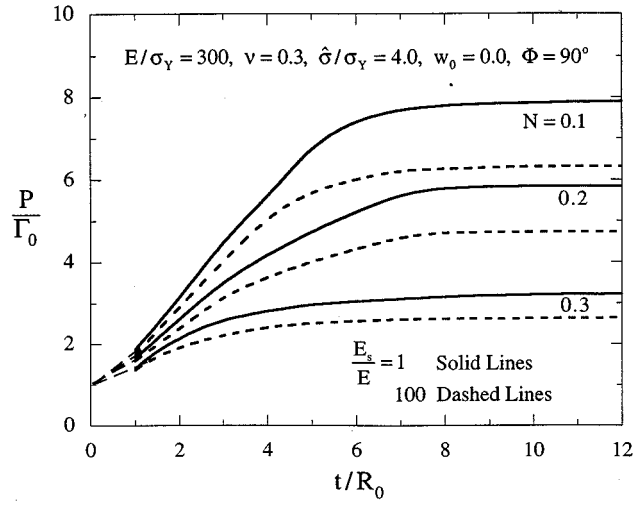

Figure 6. Influence of strain hardening index N on normalized peel force for a force acting perpendicular to the interface.

more prominent at smaller peel angles, as will be seen below. Peel tests on metal films with very strong interfaces and values of P/Γ_0 as large as 100 (Kim and Kim, 1989) display a pronounced peak at intermediate film thicknesses. The beam model of Kim and Kim (1989) predicts a peak peel force at roughly comparable values of normalized thickness.

The effect of the strain hardening index N of the film is displayed in Figure 6 for the case $w_0 = 0$. Otherwise, the parameters specifying the film/substrate system are the same as those in Figure 4. Strain hardening elevates crack tip stresses and, accordingly, makes it possible to attain a given interface strength $\widehat{\sigma}$ at a reduced peel force. It also increases the moment experienced near the tip at a given peel force. The relative effect is largest for thicker films with the highest levels of plastic dissipation.

Of all the parameters, the interface strength $\widehat{\sigma}$ has the most influence on ratio P/Γ_0, as seen in Figure 7. Curves are shown for two ratios of film to substrate moduli and three strain hardening indices. The curves are all for the case $w_0 = 0$, and they are computed with $t/R_0 =$

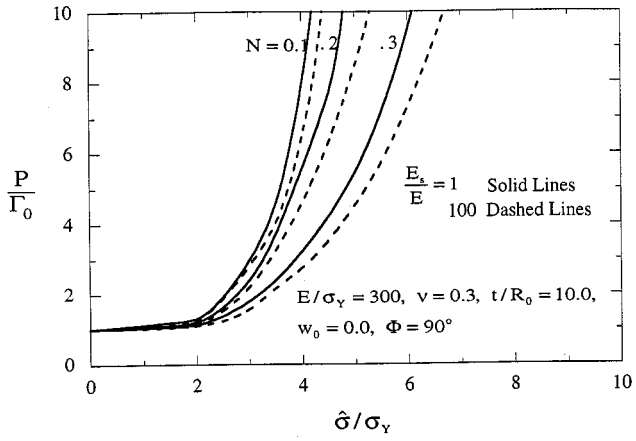

Figure 7. Dependence of the peel force on the interface strength for various levels of strain hardening for $t/R_0 = 10$. The force acts perpendicular to the interface.

10 corresponding to films that are sufficiently thick to lie near the asymptote in Figures 4 and 5. The normalized interface strength $\widehat{\sigma}/\sigma_Y$ determines the extent to which the peel force exceeds the interface work of fracture Γ_0. When $\widehat{\sigma}/\sigma_Y$ is less than about 2, plastic dissipation is nearly negligible compared to Γ_0. Local stress levels at the interface crack tip are low and induce relatively little plastic straining. This is the range of interface strengths for which the peel force is essentially the interface work of adhesion for all film thicknesses. Plastic dissipation becomes an increasingly large fraction of the total work of fracture for values of $\widehat{\sigma}/\sigma_Y$ larger than 2, depending also on N. Figure 7 drives home the central theme of this paper: the peel force scales with the work of interface adhesion, but the extent to which the peel force exceeds the work of adhesion depends primarily on the normalized interface strength. Qualitatively, these trends are similar to those found by Tvergaard and Hutchinson (1992, 1993) for the ratio the total work of fracture to the work of the fracture process for mode I crack propagation in homogeneous metals and as well as for mixed mode interface fracture under small scale yielding. In those studies, an embedded fracture process model with the traction-separation law (2.3) was also employed to represent the fracture process on the extended crack plane or on the interface.

To complete the set of results for peeling under a normal force, the residual curvature κ_0 (4.4) emerging from the crack tip region (and prior to reversed plastic bending) and the opening angle α under load measured at the interface crack tip are presented. Curves of $Et\kappa_0/[\sigma_Y(1-\nu^2)]$ as a function of t/R_0 are plotted in Figure 8 for the same set of film/substrate parameters used in plotting Figures 4 and 5. The companion plots for the crack opening angle are given in Figure 9. The opening profile of a crack near its tip in steady-state propagation can be closely approximated by the angle the separated film surface makes with substrate surface, with due account for the fact that the opening displacement at the tip itself is at the critical separation value $\delta_n(0)$ given by the traction-separation law (2.3). An effective definition can be made in terms the crack face opening $\delta_n(r)$ a small distance r behind the tip according to

$$\tan\alpha = \frac{\delta_n(r) - \delta_n(0)}{r}. \tag{5.1}$$

In the present study we have taken $r = t$. Further discussion of α is deferred to the next section.

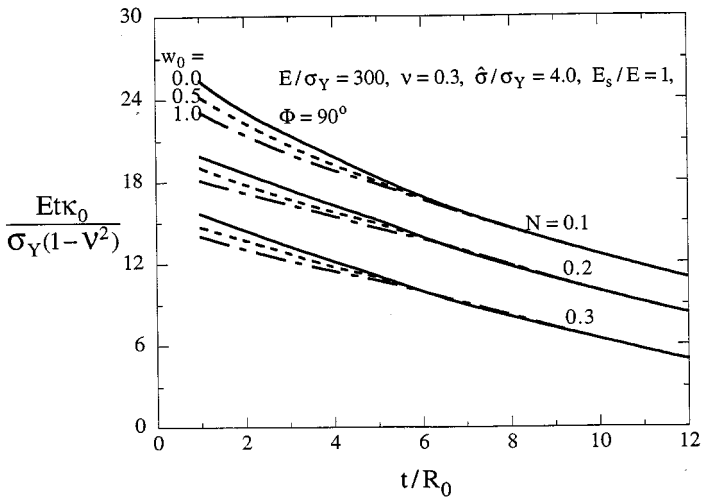

Figure 8. Variation of residual curvature κ_0 emerging from the active plastic zone at the interface crack tip as a function of film thickness for a moderately strong interface, $\widehat{\sigma}/\sigma_Y = 4$.

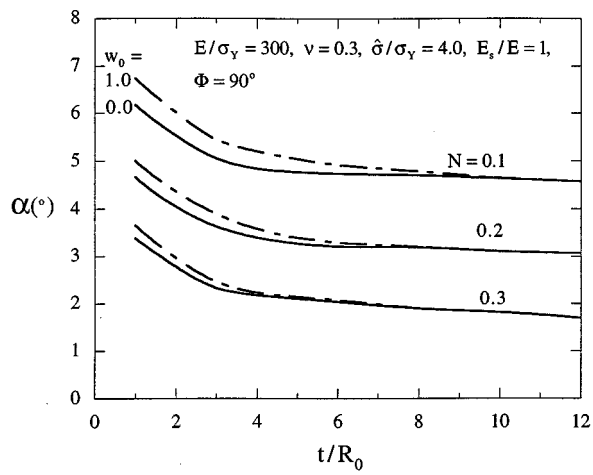

Figure 9. Variation of crack tip opening angle α at the interface crack tip as a function of film thickness for a moderately strong interface $\widehat{\sigma}/\sigma_Y = 4$.

5.2. THE ROLE OF THE PEEL ANGLE Φ

Curves of the normalized peel force as a function of film thickness are shown in Figure 10 for four peel angles. The parameters characterizing the system are the same as those in Figure 4(a). If plasticity makes a significant contribution to the total work of fracture, then decreasing the peel angle decreases $P(1 - \cos\Phi)$ but increases the peel force magnitude P. For peel angles less than about 60°, a peak in the peel force exists at an intermediate film thickness (about $t/R_0 = 6$ for the case shown). The peak is even more prominent for larger values of w_0, corresponding to less relative reversed plastic bending.

The dependence of $P(1 - \cos\Phi)/\Gamma_0$ on the normalized interface strength $\widehat{\sigma}/\sigma_Y$ is displayed in Figure 11 for four peel angles ranging from 20° to 90°. These results were computed for relatively thick films ($t/R_0 = 10$), corresponding fairly closely to the asymptote for large t/R_0. The trend with interface strength is similar to that discussed for the normal peel force.

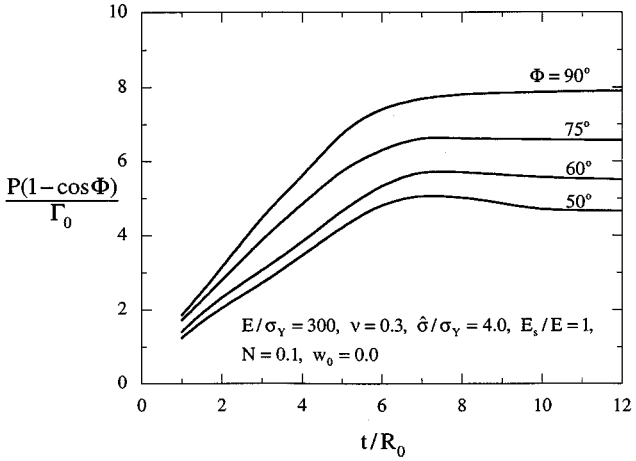

Figure 10. Normalized peel force versus film thickness for four peel angles Φ for a moderately strong interface with $\widehat{\sigma}/\sigma_Y = 4$.

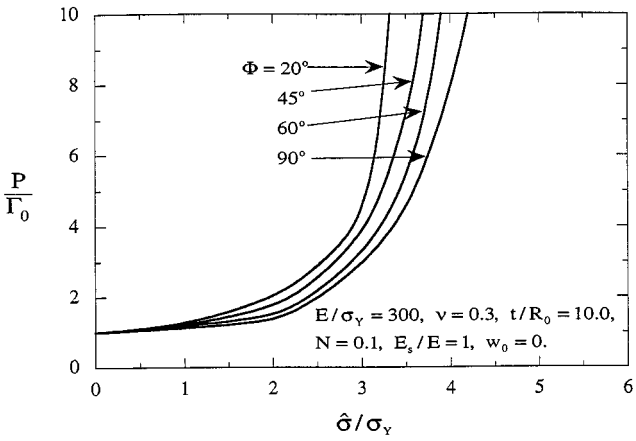

Figure 11. Normalized peel force versus interface strength for four peel angles Φ for $t/R_0 = 10$.

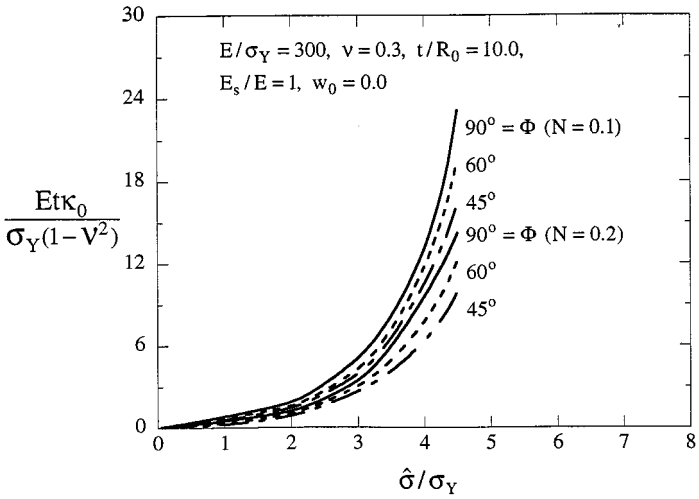

Figure 12. Residual curvature κ_0 emerging from the active plastic zone at the interface crack tip as a function of interface strength for various peel angles and strain hardening levels for $r/R_0 = 10$.

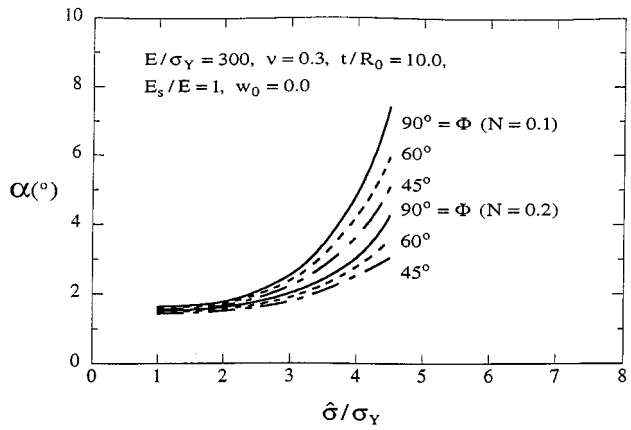

Figure 13. Crack tip opening angle α at the interface crack tip as a function of interface strength for various peel angles and strain hardening levels for $t/R_0 = 10$.

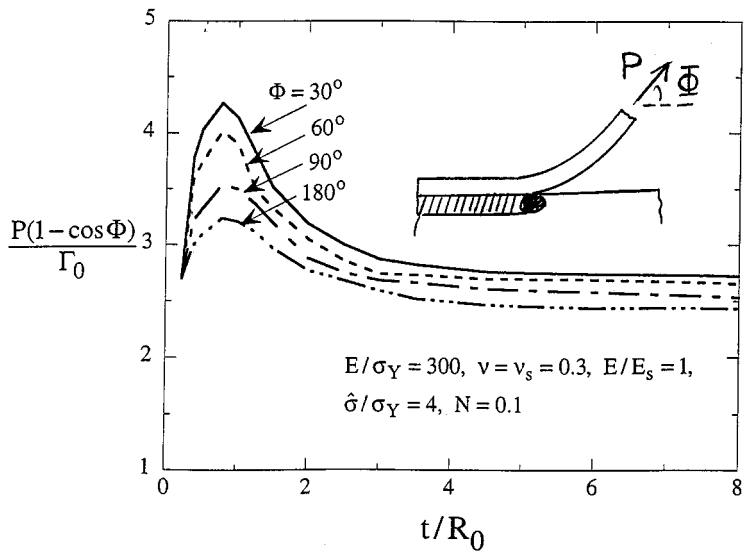

Figure 14. An elastic film peeled from an elastic–plastic substrate with yield stress σ_Y and strain hardening exponent $N = 0.1$. Normalized peel force versus film thickness for four peel angles Φ for a moderately strong interface with $\widehat{\sigma}/\sigma_Y = 4$.

It can be seen, however, that the macroscopic work of fracture, $P(1 - \cos\Phi)$, decreases with decreasing peel angle at a given interface strength, with plasticity making less of a contribution. The peel force itself P is larger at a given interface strength, the smaller is the peel angle. The residual curvature emerging from the tip region κ_0 and the opening angle α are plotted as functions of the normalized interface strength in Figures 12 and 13 for three peel angles and two levels of strain hardening, again for normalized film thickness, $t/R_0 = 10$. The trend of these quantities with interface strength is similar to that of the peel force itself. At low interface strength, both quantities are independent of $\widehat{\sigma}$, Φ and N. As $\widehat{\sigma}/\sigma_Y$ increases, κ_0 and α increase sharply and become dependent on Φ and N.

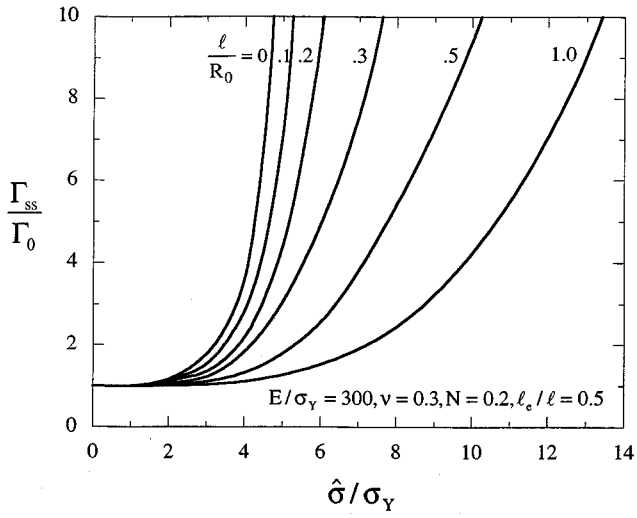

Figure 15. Influence of length parameter ℓ in strain gradient plasticity on the ratio of the total work of fracture to the work of the fracture process Γ_{ss}/Γ_0 versus normalized peak separation stress $\widehat{\sigma}/\sigma_Y$ for mode I, plane strain crack growth in a homogeneous elastic–plastic solid (Wei and Hutchinson, 1997b).

5.3. Steady-state peeling of an elastic film bonded to an elastic–plastic substrate

The model and numerical solution method applies equally well to the case where the yield strength of the film is sufficiently high such that plasticity occurs only in the substrate. Now, let σ_Y denote the yield stress of the substrate and assume that (3.1) governs substrate tensile behavior (with E replaced by E_s). The length quantity R_0 is still defined by (3.3), but with E replaced by E_s. Calculation of P/Γ_0 is more straight forward in this case because the active plastic zone in the substrate is confined to the interface crack tip and complications arising from multiple yielding regions in the film are absent. Curves of $P(1-\cos\Phi)/\Gamma_0$ as a function of t/R_0 are displayed for four peel angles in Figure 14 for the case where the film and substrate have identical elastic properties and the normalized interface strength is $\widehat{\sigma}/\sigma_Y = 4$. When the film is elastic, the plastic zone in the substrate does not shrink to zero when t becomes small and the limiting work of fracure does not approach Γ_0. A distinct peak in the peel force occurs at $t/R_0 \cong 1$; small scale yielding conditions are rapidly approached as t/R_0 increases. The ratio $P(1-\cos\Phi)/\Gamma_0$ depends only weakly on the peel angle in the small scale yielding limit implying that there is relatively little variation in mode mixity on the peel angle.

6. Implications and limitations of the model

6.1. Implications

Aside from its apparent simplicity and popularity, the peel test does not provide an easy means of determining the interface adhesion energy Γ_0, except under conditions where plastic dissipation is negligible. The cohesive zone model brings out the combined roles of the two parameters characterizing the interface, Γ_0 and interface strength $\widehat{\sigma}$, in determining the peel force and the contribution of plastic deformation to the total work of fracture. The coupling

is highly nonlinear. At high interface strength, as measured by $\widehat{\sigma}/\sigma_Y$, plastic dissipation can constitute a large fraction of the total work of fracture, such that the peel force is many times Γ_0. The model provides a computational means of partitioning the total work of fracture into the interface adhesion energy and plastic dissipation. As a practical matter, however, the task of backing out the adhesion energy from peel test data remains a major challenge.

The peel force necessarily scales with the interface adhesion energy, but a dependence on Γ_0 also enters through R_0 in (3.3) via the normalized film thickness parameter t/R_0. The film yield strength comes into play through R_0 and, most significantly, through the normalized interface strength, $\widehat{\sigma}/\sigma_Y$. In prior modeling efforts, other less fundamental quantities have been surrogate to the interface strength itself, such as the crack tip opening angle α. Nevertheless, it is clear from the numerical results presented here that the opening angle may be a useful alternative indicator of interface strength, in the sense that the larger is $\widehat{\sigma}/\sigma_Y$, the larger is α. From an observational perspective, the crack tip opening angle is far more assessable than the interface strength. Nevertheless, the two quantities are not equivalent. This is highlighted by the fact that the peel force *decreases* with increasing substrate to film modulus E_s/E at fixed $\widehat{\sigma}$, while the peel force *increases* with increasing E_s/E at fixed α (Kim et al., 1989).

The present model reveals that $P(1-\cos\Phi)/\Gamma_0$ asymptotes to a constant value for films of sufficiently large thickness. It has been noted that this is a small scale yielding limit in the sense that the active plastic zone has a height that is small compared to the film thickness. Moreover, the active plastic zone is confined to the interface crack tip and reversed plastic bending does not occur in this limit such that the macroscopic work of fracture is identical to that for an interface crack under small scale yielding at the same mode mixity. The elevation of the peel force over the adhesion energy depends on the other parameters of system, and in particular on the interface strength. Models which represent the entire film by a beam, such as those of Kim and Kim (1988) and Kim et al. (1989), are unable to capture the elevation of the peel force due to plasticity in the limit of thick films. They predict that $P(1-\cos\Phi)/\Gamma_0$ approaches unity as t/R_0 becomes large (cf. Kim and Kim, 1988). A full 2D analysis of the crack tip region such as that employed in the present approach is required to delineate role of plastic dissipation in this important limit.

6.2. Limitations

As it stands, the model is limited to systems whose normalized interface strength $\widehat{\sigma}/\sigma_Y$ is not larger than about 4 to 6, depending on strain hardening (cf. Figure 7). Larger values of $\widehat{\sigma}/\sigma_Y$ would be expected for metal films which bond strongly to ceramic substrates (cf. Kim et al., 1989), and possibly even for certain classes of polymer films bonded to metal or ceramic substrates. The conventional plasticity theory employed in the model (J_2 flow theory) does not give rise to sufficient stress elevation at the crack tip to produce separation when the normalized interface strength is larger than about 4 to 6, corresponding to values of $P(1-\cos\Phi)/\Gamma_0$ larger than about 10 to 20. As it stands, the model predicts that peeling will not take place when the interface is very strong. For metals, there are compelling reasons to believe that conventional plasticity theory significantly underestimates hardening and stresses when the gradients of plastic strain are large as, for example, at a crack tip (Fleck and Hutchinson, 1997). More and more experimental evidence is accruing indicating that, when nonuniform deformation occurs on the micron scale, elevations in tractions occur which are several times those observed at larger scales at equivalent strain levels. Stress elevation fosters interface separation at the tip of a crack on a strong interface.

A quantitative study of the effect of stress elevation on plane strain, Mode I crack growth in homogeneous metals was carried out by Wei and Hutchinson (1997b) using the same type of cohesive zone model employed here. However, in place of J_2 flow theory, these authors used a strain gradient theory of plasticity (Fleck and Hutchinson, 1997) which incorporates a length parameter ℓ characterizing the scale at which strain gradient hardening becomes important. Figure 15, from Wei and Hutchinson (1997), displays a set of results for the ratio of the total work of fracture Γ_{ss} to the work of the fracture process Γ_0 as a function of normalized interface strength for various levels of the new nondimensional length parameter ℓ/R_0. These results apply to steady-state propagation in small scale yielding. The reference length R_0 is the same as defined here in (3.3). The limiting curve for $\ell/R_0 = 0$ corresponds to the behavior predicted using the conventional plasticity theory J_2 flow theory. Values of ℓ/R_0 in the range from 0.1. to 1 produce crack tip stress elevation and give rise to crack propagation at much larger normalized separation strengths $\widehat{\sigma}/\sigma_Y$ than can be encompassed by the conventional plasticity theory.

The implications of these results for strong interfaces become apparent when one considers values of the reference length R_0. For relatively strong metal/ceramic interfaces failing by atomic decohesion, representative values of R_0 in (3.3) typically fall in the range from about one tenth to several microns. From available experimental data, the length parameter ℓ appears to be on the order of a micron for many metals (Fleck and Hutchinson, 1997). Thus, it is evident from Figure 15 that strain gradient effects should have a profound influence on the relationship between the total work of fracture and the work of adhesion for strong metal/ceramic interfaces. For less strong interfaces and for systems for which ℓ/R_0 is small, the present model based on conventional plasticity theory should be adequate.

Acknowledgment

This work was supported in part by the ONR through grant N00014-96-10059, by the NSF through grant NSF-CMS-96-34632, and by the Division of Engineering and Applied Sciences, Harvard University.

References

Dean R.H. and Hutchinson, J.W. (1980). Quasi-static steady crack growth in small scale yielding. In *Fracture Mechanics*, ASTM STP 700, American Society for Testing Materials, 383–405.

Fleck, N.A. and Hutchinson, J.W. (1997). Strain gradient plasticity. *Advances in Applied Mechanics* (Edited by J.W. Hutchinson and T.Y. Wu) **33**, 295–361.

Kim, J., Kim, K.-S. and Kim, Y.H. (1989). Mechanical effects of peel adhesion test. *Journal of Adhesion Science and Technology* **3**, 175–187.

Kim, K.-S. and Aravas, N. (1988). Elasto–plastic analysis of the peel test. *International Journal of Solids and Structures* **24**, 417–435.

Kim, K.-S. and Kim, J. (1988). Elasto–plastic analysis of the peel test for thin film adhesion. *Journal of Engineering Materials and Technology* **110**, 266–273.

Kinloch, A.J., Lau, C.C. and Williams, J.G. (1994). The peeling of flexible laminates. *International Journal of Fracture* **66**, 45–70.

Parks, D.M., Lam, P.S. and McMeeking, R.M. (1981). Some effects of inelastic constitutive models on crack tip fields in steady crack growth. *Advances in Fracture Research* (Edited by D. Francois), Pergamon Press, **5**, 2607–2614.

Tvergaard, V. and Hutchinson, J.W. (1992). The relation between crack growth resistance and fracture process parameters in elastic–plastic solids. *Journal of the Mechanics and Physics of Solids* **40**, 1377–1397.

Tvergaard, V. and Hutchinson, J.W. (1993). The influence of plasticity on mixed mode interface toughness. *Journal of the Mechanics and Physics of Solids* **41**, 1119–1135.

Wei, Y. and Hutchinson, J.W. (1997a). Nonlinear delamination mechanics for thin films. *Journal of the Mechanics and Physics of Solids* **45**, 1137–1159.

Wei, Y. and Hutchinson, J.W. (1997b). Steady-state crack growth and work of fracture for solids characterized by strain gradient plasticity. *Journal of the Mechanics and Physics of Solids* **45**, 1253–1273.